Article

Curvature Invariants for Lorentzian Traversable Wormholes

Brandon Mattingly [1,2,*] , **Abinash Kar** [1,2] , **William Julius** [1,2] , **Matthew Gorban** [1,2] ,
Cooper Watson [1,2] , **MD Ali** [1,2] , **Andrew Baas** [1,2] , **Caleb Elmore** [1,2] , **Bahram Shakerin** [1,2] ,
Eric Davis [1,3] and **Gerald Cleaver** [1,2]

1   Early Universe, Cosmology and Strings (EUCOS) Group, Center for Astrophysics, Space Physics and
    Engineering Research (CASPER), Baylor University, Waco, TX 76798, USA; Abinash_Kar@baylor.edu (A.K.);
    William_Julius1@Baylor.edu (W.J.); Matthew_Gorban1@baylor.edu (M.G.); Cooper_Watson@Baylor.edu
    (C.W.); mali54@hawk.iit.edu (M.D.A.); Andrew_Baas@Baylor.edu (A.B.); Cale5895@gmail.com (C.E.);
    Bahram.shakerin@gmail.com (B.S.); Eric_W_Davis@Baylor.edu (E.D.); gerald_cleaver@baylor.edu (G.C.)
2   Department of Physics, Baylor University, Waco, TX 76798, USA
3   Institute for Advanced Studies at Austin, 11855 Research Blvd., Austin, TX 78759, USA
*   Correspondence: Brandon_Mattingly@Baylor.edu

check for updates

Abstract: The curvature invariants of three Lorentzian wormholes are calculated and plotted in this
paper. The plots may be inspected for discontinuities to analyze the traversability of a wormhole.
This approach was formulated by Henry, Overduin, and Wilcomb for black holes (Henry et al., 2016).
Curvature invariants are independent of coordinate basis, so the process is free of coordinate mapping
distortions and the same regardless of your chosen coordinates (Christoffel, E.B., 1869; Stephani, et al.,
2003). The four independent Carminati and McLenaghan (CM) invariants are calculated and the
nonzero curvature invariant functions are plotted (Carminati et al., 1991; Santosuosso et al., 1998).
Three traversable wormhole line elements analyzed include the (i) spherically symmetric Morris and
Thorne, (ii) thin-shell Schwarzschild wormholes, and (iii) the exponential metric (Visser, M., 1995;
Boonserm et al., 2018).

Keywords: traversable wormhole; curvature invariant; Carminati and McLenaghan; general relativity

PACS: 04.20.-q; 04.20.Cv; 02.40.-k

1. Introduction

Lorentzian traversable wormholes were first described by Kip Thorne and collaborators who
used Einstein's general relativistic field equations to explore the possibility of faster-than-light (FTL)
interstellar spaceflight without violating special relativity [1,2]. Earlier studies demonstrated the
possibility of traversable wormholes in general relativity [3,4]. A Lorentzian traversable wormhole is a
topological opening in spacetime which manifests traversable intra-universe and/or inter-universe
connections, as well as possible different chronological connections between distant spacetime points.
The condition for a Lorentzian wormhole to be traversable is that it is free of both event horizons
and singularities [5]. Such a wormhole is fully traversable in both directions, geodesically complete,
and possesses no crushing gravitational tidal forces found anywhere inside. Consequently, Lorentzian
traversable wormholes are unlike the nontraversable Schwarzschild wormhole, or Einstein–Rosen
bridge, associated with eternal black holes in the maximally extended version of the Schwarzschild
metric. Exotic matter, which violates the point-wise and averaged energy conditions, is required to
open and stabilize a Lorentzian traversable wormhole. A comprehensive technical overview of this
subject is found in [5].

Previous studies of Lorentzian traversable wormholes rely on either calculating the elements of the Riemann curvature tensor, R^i_{jkl}, to "observe" the effects of the wormhole's spacetime curvature on photons and matter moving through it or by embedding diagrams. However, the R^i_{jkl} cannot be calculated in an invariant manner because it is a function of the chosen coordinates [6]. Analysis of R^i_{jkl} can be misleading because a different choice of coordinate basis will result in different tensor components. These coordinate mapping distortions arise purely as an artifact of the coordinate choice. Embedding diagrams offer a narrow view of the spacetime manifold. In [1], the embedding diagrams depicts the wormhole geometry along just an equatorial ($\theta = \frac{\pi}{2}$) slice through space at a specific moment in time. The embedding diagram only offers a limited view of the physics involved in the wormhole. Curvature invariants allow a manifestly coordinate invariant characterization of certain geometrical properties of spacetime [7]. The best way to illustrate wormhole spacetimes without such issues is to plot their independent curvature invariants to provide proper visualization of any hidden surprises.

Christoffel proved that scalars constructed from the metric and its derivatives must be functions of the metric itself, the Riemann tensor and its covariant derivatives [8]. Curvature invariants are scalar products of Riemann, Ricci, or Weyl tensors, or their covariant derivatives. Curvature invariants are of particular interest in general relativity for identifying intrinsic singularities in spacetimes, classifying the Petrov type of the Weyl tensor and the Segre type of the trace-free Ricci tensor, and studying the equivalence problem [7,9–15]. The study of curvature invariants is a subject of recent black hole research with a priority on locating their horizons [16–21]. Specific curvature invariants of certain wormholes have been calculated to locate any singularities and horizons, but a complete set has not been presented and calculated [22–24]. The set of Carminati and McLenaghan (CM) invariants are of lowest degree and contains a minimal independent set for any Petrov or Segre types [25]. For class B warped product spacetimes[1], four of the CM invariants, R, r_1, r_2, and w_2, are needed to satisfy the syzygies[2] [27]. In this paper, the CM curvature invariants of popular wormholes will be plotted and the geometrical properties analyzed.

In [16], Henry et al. computed and plotted a number of independent curvature invariants for the hidden interiors of Kerr–Newman black holes. They produced visually stunning 3D plots which revealed the surprisingly complex nature of spacetime curvature in Kerr–Newman black hole interiors. Their work motivated the present authors to undertake a similar study for the case of Lorentzian traversable wormholes. Reported here are the computations and 3D plots for three selected Lorentzian traversable wormholes that are described in [5,22]: (i) the Morris and Thorne (MT) wormhole, (ii) the thin-shell Schwarzschild wormhole, and (iii) the exponential metric. The thin-shell flat-face (TS) wormhole was also analyzed, but all of its invariants were trivial as they were identically zero.

2. Method to Compute the Invariants

The CM curvature invariants can be calculated from any given line element. From the line element, identify the metric g_{ij} with the indices $\{i, j, k, l\}$ ranging from $\{0, n-1\}$, where n is the number of spacetime dimensions. In this paper, a basis or a tetrad will be chosen for each metric. It is emphasized that the scalar invariants are independent of the choice of coordinates in a tetrad. A different choice of coordinates for each spacetimes' tetrad will result in the same invariants plotted in this paper. From the metric, the Ricci scalar R, the trace-free Ricci tensor S_{ij} and the Weyl tensor C_{ijkl} can be calculated [10].

---

[1] Warped products of class B are line elements of the form $ds^2 = ds^2_{\Sigma_1}(u,v) + C(x^\gamma)^2 ds^2_{\Sigma_2}(\theta,\phi)$ subject to the restriction $C(x^\gamma)^2 = r(u,v)^2 e(\theta,\phi)^2$. Class B_1 spacetimes include all spherical, planar, and hyperbolic spacetimes and contain all spacetime line elements considered in this paper [26].

[2] The syzygies reveal either all independent irreducible algebraic relations among the set of invariants or that no set exists [9].

The literature defines fourteen curvature invariants, but the total rises to seventeen when certain nondegenerate cases are taken into account [7,25]. The four CM invariants as required by the syzygies are [27]:

$$R = g_{ij}R^{ij}, \tag{1}$$

$$r_1 = \frac{1}{4}S_i^j S_j^i, \tag{2}$$

$$r_2 = -\frac{1}{8}S_i^j S_k^i S_j^k, \tag{3}$$

$$w_2 = -\frac{1}{8}\bar{C}_{ijkl}\bar{C}^{ijmn}\bar{C}^{kl}_{mn}. \tag{4}$$

The full solutions to the wormhole metrics studied herein were found using Wolfram Mathematica 10.4®.

3. Morris and Thorne Wormhole

The MT wormhole is defined by a spacetime, which is spherically symmetric and Lorentzian. The spacetime describes the required traversable wormhole geometry. In the standard Schwarzschild coordinates [1], the line element is:

$$ds^2 = -e^{2\phi^{\pm}(r)}dt^2 + \frac{dr^2}{\left(1 - \frac{b^{\pm}(r)}{r}\right)} + r^2(d\theta^2 + sin^2\theta d\varphi^2). \tag{5}$$

The tetrad for the MT line element uses the spherical coordinates (r: with circumference $= 2\pi r$; $0 \leq \theta \leq \pi$; $0 \leq \varphi \leq 2\pi$), and ($-\infty < t < \infty$) is the proper time of a static observer. $\phi^{\pm}(r)$ is the freely specifiable redshift function that defines the proper time lapse through the wormhole throat. $b^{\pm}(r)$ is the freely specifiable shape function that defines the wormhole throat's spatial (hypersurface) geometry. The $\pm$ indicates the side of the wormhole. The throat described by Equation (5) is spherical. A fixed constant, r_0, is chosen to define the radius of the wormhole throat such that $b^{\pm}(r_0) = r_0$, which is an isolated minimum. Two coordinate patches of the manifold are then joined at r_0. Each patch represents either a different part of the same universe or another universe, and the patches range from $r_0 \leq r < \infty$. The condition that the wormhole is horizon free requires that $g_{tt} = -e^{2\phi^{\pm}(r)} \neq 0$. This implies that $|\phi^{\pm}(r)|$ must be finite everywhere [5,28]. The use of Schwarzschild coordinates in Equation (5) leads to more efficient computations of the Riemann and Ricci curvature tensors, the Ricci scalar, and all four invariants.

The four CM invariants for the Morris-Thorne wormhole are

$$R = \frac{1}{r^2}\left(b'\left(r\Phi' + 2\right) + 2r\left(b - r\right)\Phi'' - 2r\left(r - b\right)\Phi'^2 + (3b - 4r)\Phi'\right), \tag{6}$$

$$\begin{aligned}r_1 = \frac{1}{16r^6}(r^2(b'^2\left(r^2\Phi'^2 + 2\right) - 4rb'\Phi'\left(r^2\Phi'' + r^2\Phi'^2 - 2\right) + 4r^2(r^2\Phi''^2 + r^2\Phi'^4 + 2\Phi'^2\left(r^2\Phi'' + 1\right))) \\ - 2rb(b'\left(-2r^3\Phi'^3 + \Phi'\left(6r - 2r^3\Phi''\right) + r^2\Phi'^2 + 2\right) + 2r(2r^3\Phi'^4 + 2\Phi'^2\left(2r^3\Phi'' + r\right) \\ + 2r\Phi''\left(r^2\Phi'' - 1\right) - r^2\Phi'^3 + \Phi'\left(2 - r^2\Phi''\right))) \\ + b^2(4r^4\Phi''^2 + 4r^4\Phi'^4 - 4r^3\Phi'^3 - 8r^2\Phi'' - 4r\Phi'\left(r^2\Phi'' - 3\right) + \Phi'^2\left(8r^4\Phi'' + r^2\right) + 6)),\end{aligned} \tag{7}$$

$$r_2 = -\frac{3}{64r^9}\left(b\left(2r\Phi' + 1\right) - r\left(b + 2r\Phi'\right)\right)^2(r^2\left(b'\Phi' - 2r\left(\Phi'' + \Phi'^2\right)\right) + b\left(2r^2\Phi'' + 2r^2\Phi'^2 - r\Phi' - 2\right)), \tag{8}$$

$$w_2 = \frac{1}{144r^9}\left(r\left(b'\left(1 - r\Phi'\right) + 2r\left(r\Phi'' + r\Phi'^2 - \Phi'\right)\right) - b\left(2r^2\Phi'' + 2r^2\Phi'^2 - 3r\Phi' + 3\right)\right)^3. \tag{9}$$

All the invariants are nonzero and depend only on the radial coordinate, r, implying they are spherically symmetric. The invariants are plotted in Figure 1 after selecting a redshift function of $\phi(r) = 0$ and the shape function of

$$b(r) = 2GM\left(1 - e^{r_0 - r}\right) + r_0 e^{r_0 - r}. \tag{10}$$

These functions satisfy the constraints on the asymptotic behavior and continuity at the wormhole's throat [5]. At a distant greater than 0.5 r_0, all the figures are asymptotically flat. For $r \to 0$, the figures diverge to infinity. The divergence at $r = 0$ is not pathological as the radial coordinate r has a minimum $r_0 > 0$ at the wormhole's throat. Thus, a traveler passing through the wormhole would not experience any divergence. Any tidal forces on the traveler would be minimal. Consequently, the MT wormhole would be traversable as indicated by the included invariant plots.
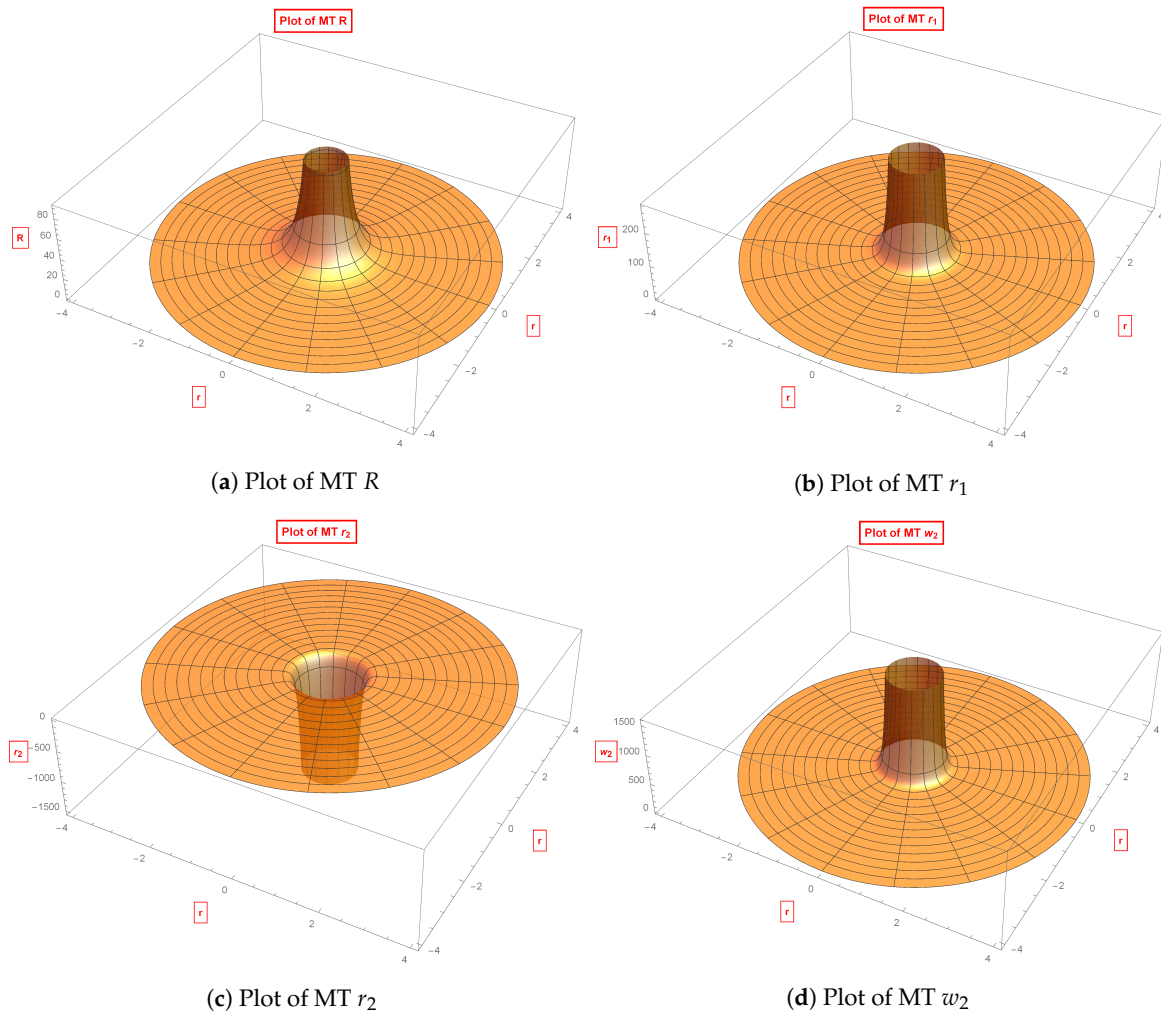

(**a**) Plot of MT R

(**b**) Plot of MT r_1

(**c**) Plot of MT r_2

(**d**) Plot of MT w_2

Figure 1. Plots of the nonzero invariants for the Morris and Thorne (MT) wormhole. The plots are in radial coordinates with $r \in \{0, 4\}$. Each radial mesh line represents a radial distance of $r = 0.2\bar{6}$. $G = M = 1$ were normalized for simplicity and $r_0 = 2$ was chosen as the throat. Notice the divergence at the center of each plot is completely inside the $r = 2 = r_0$ radial line. This does not affect the traversability of the wormhole.

4. Thin-Shell Schwarzschild Wormhole

A second example wormhole is the thin-shell Schwarzschild wormhole. The Schwarzschild geometry in natural units is given by the line element:

$$ds^2 = -\left(1 - \frac{2M}{r}\right) dt^2 + \frac{dr^2}{\left(1 - \frac{2M}{r}\right)} + r^2 \left(d\theta^2 + sin^2\theta d\varphi^2\right), \tag{11}$$

where M is the mass of the wormhole. The tetrad of the line element is the spherical coordinates. The thin shell formalism developed in [5] is used to construct the two sides of the wormhole. Each side is described by Equation (11). The thin-shell formalism is applied with a unit normal $n_i =$

$\left(0, \sqrt{1 - \frac{2M}{r}}, 0, 0\right)$. Regions described by $\Omega_{1,2} \equiv \left\{r_{1,2} \leq a \mid a > \frac{3M}{2}\right\}$ are removed from the two spacetimes leaving two separate and incomplete regions with boundaries given by the time-like hypersurfaces $\partial\Omega_{1,2} \equiv \left\{r_{1,2} = a \mid a > \frac{3M}{2}\right\}$. The boundaries $\partial\Omega_1 = \partial\Omega_2$ at the wormhole throat of $r = a$ are identified and connected. The boundary at $a = \frac{3M}{2}$ is chosen to satisfy the Einstein equations and equation of state in [5]; however, an event horizon is expected. The resulting spacetime manifold is geodesically complete and contains two asymptotically flat regions connected by the wormhole.

Of the four CM invariants computed for the Schwarzschild wormhole, three invariants R, r_1, and r_2 equal zero. The remaining invariant is

$$
\begin{aligned}
w_2 = &-\frac{12M^3}{r^9} + \frac{6M^2}{a^2 r^9}\sqrt{1 - \frac{2M}{a}}\left(a\left(r - 2M\right) + 2M\left(2M + 2r^3 - r\right)\right)\delta\left(r - a\right) \\
&+ \frac{12M}{a^5 r^9}\left(a - 2M\right)\left(4M^2\left(a - 2M\right)^2 + r^2\left(a - 2M\right)^2 - 4Mr\left(a - 2M\right)^2 - 2M^2 r^6\right)\delta\left(r - a\right)^2 \\
&+ \frac{8}{a^6 r^9}\left(1 - \frac{2M}{a}\right)^{3/2}\left(\left(a - 2M\right)^3\left(r - 2M\right)^3 + M^3 r^9\right)\delta\left(r - a\right)^3.
\end{aligned}
\tag{12}
$$

The w_2 invariant is broken into two main portions. The leading term of $\frac{-12M^3}{r^9}$ is the Schwarzschild black hole's w_2 invariant. The remaining portions of the function are all proportional to different powers of $\delta\left(r - a\right)$. Consequently, they contribute to the throat of the wormhole. Evaluating w_2 at the throat gives

$$
\begin{aligned}
w_2|_{r=a} = \frac{2}{a^{14}}\Big(&-6a^5 M^3 + 4a^8\left(\frac{\left(a - 2M\right)^6}{a^9} + M^3\right)\left(1 - \frac{2M}{a}\right)^{\frac{3}{2}} \\
&+ 3a^3 M^2\left(4a^3 M + a^2 - 4aM + 4M^2\right)\sqrt{1 - \frac{2M}{a}} \\
&- 6M\left(a - 2M\right)\left(2a^6 M^2 - a^4 + 8a^3 M - 24a^2 M^2 + 32aM^3 - 16M^4\right)\Big).
\end{aligned}
\tag{13}
$$

Since $w_2 \propto \frac{1}{a^{14}}$, the throat will experience greater curvature the smaller it is and vice versa.

The only nonzero invariant, w_2, is plotted in Figure 2. The mass and radius of the throat are normalized to $M = 1$ and $a = \frac{3}{2}$ in the plot. Its plot has one divergence and one discontinuity. The divergence occurs at $r = 0$, which is outside the manifold of $\Omega_{1,2}$. By the same argument for the apparent MT divergence, the first Schwarzschild divergence would not impede the traversability of the wormhole. The discontinuity occurs at $r = a = \frac{3M}{2}$ and is located at the throat where the horizons are connected by the Schwarzschild wormholes. In these invariants, it is represented by a discontinuous jump to the value in Equation (13). Since the invariants at the horizon are inversely proportional to a^{-14}, the tidal forces on a traveler is benign at the horizon, and the thin-shell Schwarzschild wormhole would be traversable.
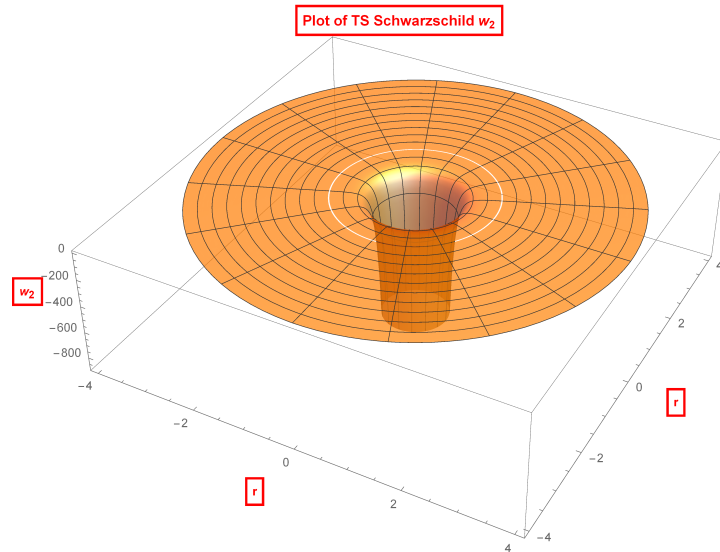
Figure 2. Plot of Schwarzschild w_2. The plot is in radial coordinates with $r \in \{0, 4\}$. Each mesh line represents a radial distance of 0.5. The δ-function can be seen as a thin discontinuity at $r = 32$ and its value is recorded in Equation (13).

5. The Exponential Metric

The exponential metric was demonstrated recently in [22] to have a traversable wormhole throat. In natural units, its line element is

$$ds^2 = -e^{\frac{-2M}{r}} dt^2 + e^{\frac{+2M}{r}} \left\{ dr^2 + r^2 \left(d\theta^2 + \sin^2\theta d\varphi^2 \right) \right\}, \tag{14}$$

where M is the mass of the wormhole. The tetrad utilizes the spherical coordinates. It has a traversable wormhole throat at $r = M$. The area of the wormhole is a concave function with a minima at the throat where it satisfies the "flare out" condition. It does not have a horizon since $g_{tt} \neq 0$ for all $r \geq 0$. The region $r < M$ on the other side of the wormhole is an infinite volume "other universe" that exhibits an "underhill effect" where time runs slower since $e^{\frac{-2M}{r}} > 0$ in this region.

Computing the four curvature invariants for the exponential metric with Wolfram Mathematica $10.4^{\circledR}$ gives

$$R = -\frac{2M^2}{r^4} e^{-\frac{2M}{r}}, \tag{15}$$

$$r_1 = \frac{3M^4}{4r^8} e^{-\frac{4M}{r}}, \tag{16}$$

$$r_2 = \frac{3M^6}{8r^{12}} e^{-\frac{6M}{r}}, \tag{17}$$

$$w_2 = -\frac{32M^3(2M - 3r)^3}{9r^{12}} e^{-\frac{6M}{r}}. \tag{18}$$

They are all nonzero and depend only the radial coordinate r implying spherical symmetry. In addition, they are finite at the throat $r = M$ and go to zero as $r \to \infty$ in accordance with [22]. w_2 and R have a minima near the throat, while r_1 and r_2 have a maxima. The plots are finite everywhere and completely connected confirming the lack of a horizon. The encountered tidal forces would be minimal. It can be concluded that the exponential metric represents a traversable wormhole.

6. Conclusions

This paper demonstrates how to compute and plot the curvature invariants of various wormhole line elements. The curvature invariants reveal the entire wormhole spacetime manifold and whether the

wormhole is traversable or not. As examples, plotting the CM curvature invariants of the (i) spherically symmetric MT, (ii) thin-shell Schwarzschild, and (iii) exponential metric wormholes showed they are traversable in agreement with [1,2,5]. The scalar polynomial invariants of the MT wormhole were found to be nonzero and are plotted in Figure 1a–d. A divergence is found in all four, but it does not affect the wormhole's traversability since the divergence is outside the physical range of the radial coordinate, $r \in (r_0, \infty)$. For the thin-shell Schwarzschild wormhole, w_2 is found to be the single nonzero invariant. As plotted in Figure 2, it has a divergence at the center and a ring discontinuity. The divergence is outside the physical radial coordinate and can be safely ignored. The ring discontinuity represents a jump due to the δ-function from the thin-shell formalism. It is shown to be inversely proportional to a^{-14}, not affecting traversability through the wormhole. The scalar polynomial invariants of the exponential metric were found to be nonzero and were plotted in Figure 3a–d. The plots are continuous across the entire manifold and traversable.
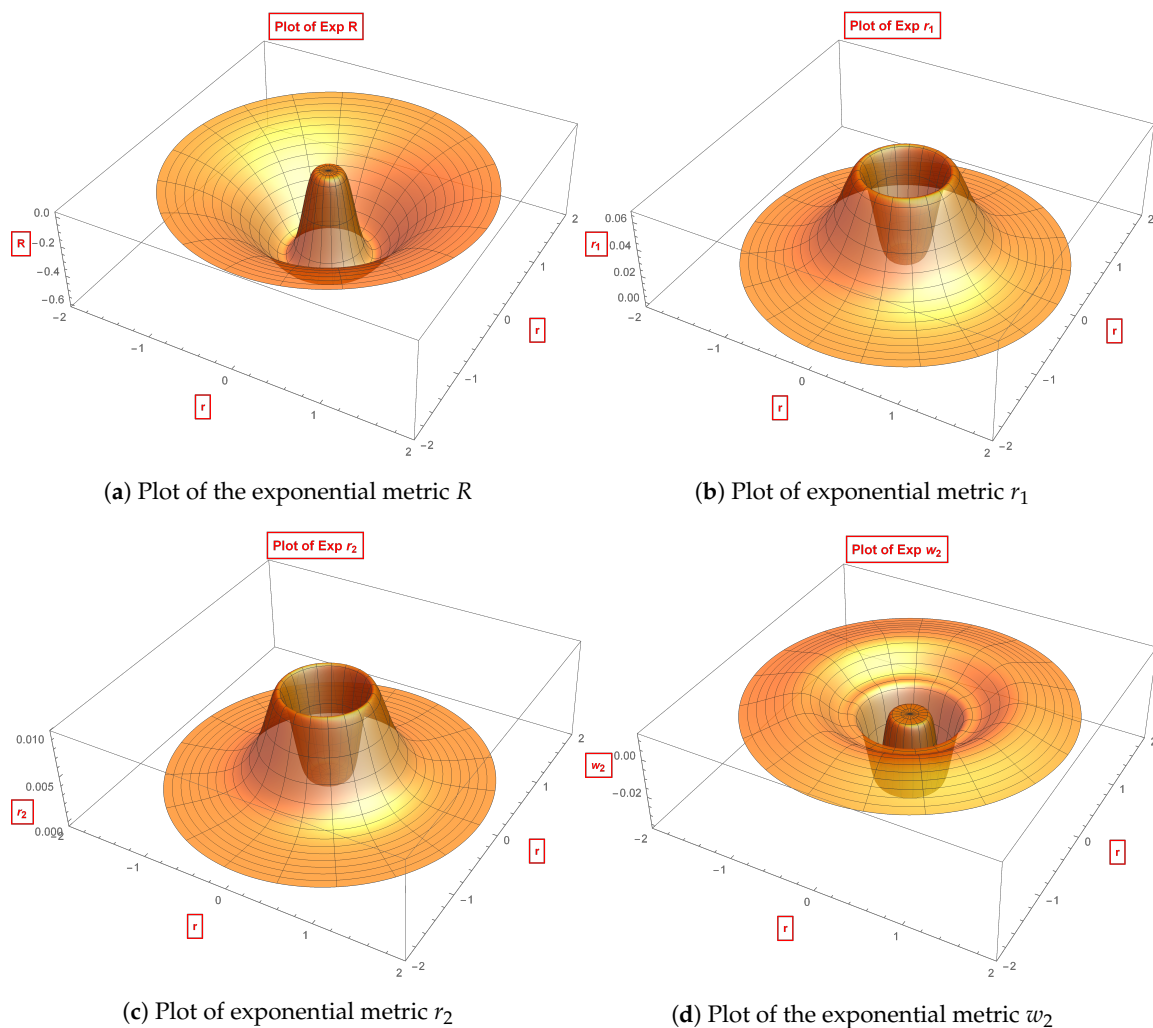

(**a**) Plot of the exponential metric R

(**b**) Plot of exponential metric r_1

(**c**) Plot of exponential metric r_2

(**d**) Plot of the exponential metric w_2

Figure 3. Plots of the nonzero invariants for the exponential metric. The plots are in radial coordinates with $r \in \{0, 1.8M\}$. Each mesh line represents a radial distance of $0.1M$. The throat begins at $r = M$.

Potentially, the ring discontinuity in the thin-shell Schwarzschild wormhole could lead to a redshift of light rays passing through the wormhole. The redshift could be used to distinguish wormholes from black holes. While significant research remains to answer traversable wormhole issues, especially with regards to the exotic mass requirements and understanding averaged null energy condition violations, the present paper hopes to establish several methods for understanding the traversal through wormholes.

Computing and plotting the invariant functions has significant advantages for the inspection of wormholes. As mentioned previously, the advantage of plotting the invariants is that they are free from coordinate mapping distortions and other artifacts of the chosen coordinates. The resulting invariants properly illustrate the entire underlying spacetime independent of the coordinate system chosen. Plotting the invariants exposes the presence of any artifacts, divergences, or discontinuities anywhere on the manifold. Once the artifacts are revealed by the invariants, they can be related mathematically to the textbook tensors. Any artifact's effect can then be analyzed based on where the curvature invariant locates it, what type of artifact the curvature invariant reveals it to be, and how the artifact may affect the object's motion based on the plots of the curvature invariant at that location. A second advantage is the relative ease with which the invariants can be plotted. Software packages exist or can be developed to calculate the textbook tensors. Then, the CM invariants can be derived from the textbook using minimal edits to the software packages. The CM invariants were chosen to be computed and plotted in this paper because they had general independence, were of lowest possible degree, and a minimal independent set for any Petrov Type and for any specific choice of the Ricci tensor [25]. It is of research interest that other choices for the set of invariants exist, such as the Cartan invariants and the Witten and Petrov invariants [7,29]. These can be also computed and plotted without difficulty, but they will be related to the CM invariants by polynomial functions [7]. Since the invariants are either scalars or pseudoscalars, they can be straightforwardly plotted and visually interpreted.

The thin-shell Schwarzschild wormhole is the most common example of a large class of wormholes. The class includes wormholes with different radii of curvature and/or masses on either side of the throats, wormholes with same or different charge, Q, on either side of the wormhole, and time-dependent wormholes. For charged wormholes, a second ring artifact at $r = Q$ is likely to exist since the metric has a singularity at that point.

A prospective future application of this work is an investigation of wormholes with throats that change dynamically over time. This implies that the ring discontinuity in the invariant functions will change as a function of time. Hence, dynamic wormholes are technically more intricate to study as compared to static wormholes. Consequently, it can be expected that the computation of a dynamic wormhole's invariants and their plots increase in difficulty and computational runtime. In a broader perspective, the calculation and plotting of curvature invariants can be made to encompass other types of FTL spaceflight such as the Alcubierre warp drive [30].

References

1. Morris, M.S.; Thorne, K.S. Wormholes in spacetime and their use for interstellar travel: A tool for teaching general relativity. *Am. J. Phys.* **1988**, *56*, 395–412. [CrossRef]
2. Morris, M.S.; Thorne, K.S.; Yurtsever, U. Wormholes, time machines, and the weak energy conditions. *Phys. Rev. Lett.* **1988**, *61*, 1446–1449. [CrossRef] [PubMed]
3. Ellis, H.G. Ether flow through a drainhole: A particle model in general relativity. *J. Math. Phys.* **1973**, *14*, 104–118. [CrossRef]
4. Bronnikov, K.A. Scalar-tensor theory and scalar charge. *Acta Phys. Pol.* **1973**, *4*, 251–266.
5. Visser, M. *Lorentzian Wormholes: From Einstein to Hawking*; AIP Press: New York, NY, USA, 1995.

6. Penrose, R.; Rindler, W. *Spinors and Space-Time*; Cambridge Monographs on Mathematical Physics; Cambridge University Press: Cambridge, UK, 1986.

7. Zakhary, E.; McIntosh, C.B.G. A Complete Set of Riemann Invariants. *Gen. Relativ. Gravit.* **1997**, *29*, 539–581. [CrossRef]

8. Christoffel, E.B. Ueber die Transformation der homogenen Differentialausdrücke zweiten Grades. *J. Angew. Math.* **1869**, *70*, 46–70.

9. Stephani, H.; Kramer D.; MacCallum, M.A.H.; Hoenselaers, C.; Herlt, E. *Exact Solutions of Einstein's Field Equations*; Cambridge Monographs on Mathematical Physics; Cambridge University Press: Cambridge, UK, 2003.

10. D'Inverno, R.C. *Introducing Einstein's Relativity*; Oxford University Press: Oxford, UK, 1992.

11. Carroll, S. *Spacetime and Geometry: An Introduction to General Relativity*, 1st ed.; Pearson Education Limited: London, UK, 2014.

12. Groen, O.; Hervik, S. *Einstein's General Theory of Relativity: With Modern Applications in Cosmology*; Springer: New York, NY, USA, 2007; p. 538.

13. Cherubini, C.; Bini, D.; Capozziello, S.; Ruffini, R. Second order scalar invariants of the Riemann tensor: Applications to black hole space-times. *Int. J. Mod. Phys. D* **2002**, *11*, 827–841. [CrossRef]

14. Coley, A.; Hervik, S.; Pelavas, N. Spacetimes characterized by their scalar curvature invariants. *Class. Quantum Gravity* **2009**, *26*, 025013. [CrossRef]

15. MacCallum, M.A.H. Spacetime invariants and their uses. *arXiv* **2015**, arXiv:1504.06857v1.

16. Henry, R.C.; Overduin, J.; Wilcomb, K. A New Way to See Inside Black Holes. *arXiv* **2016**, arXiv:1512.02762v2.

17. Baker, J.G.; Campanelli, M. Making use of geometrical invariants in black hole collisions. *Phys. Rev. D* **2000**, *62*, 127501. [CrossRef]

18. MacCallum, M.A.H. On singularities, horizons, invariants, and the results of Antoci, Liebscher and Mihich (GRG 38, 15 (2006) and earlier). *Gen. Relativ. Gravit.* **2006**, *38*, 1887–1899. [CrossRef]

19. Abdelqader, M.; Lake, K. Invariant characterization of the Kerr spacetime: Locating the horizon and measuring the mass and spin of rotating black holes using curvature invariants. *Phys. Rev. D* **2015**, *91*, 084017. [CrossRef]

20. Page, D.N.; Shoom, A.A. Local Invariants Vanishing on Stationary Horizons: A Diagnostic for Locating Black Holes. *Phys. Rev. Lett.* **2015**, *114*, 141102. [CrossRef] [PubMed]

21. Coley, A.; McNutt, D. Identification of black hole horizons using scalar curvature invariants. *Class. Quantum Gravity* **2018**, *35*, 025013. [CrossRef]

22. Boonserm, P.; Ngampitipan, T.; Simpson, A.; Visser, M. Exponential metric represents a traversable wormhole. *Phys. Rev. D* **2018**, *98*, 084048. [CrossRef]

23. Agnese, A.G.; La Camera, M. Traceless stress energy and traversable wormholes. *Nuovo Cim. B* **2002**, *117*, 647–652.

24. Korolev, R.V.; Sushkov, S.V. Exact wormhole solutions with nonminimal kinetic coupling. *Phys. Rev. D* **2014**, *90*, 124025. [CrossRef]

25. Carminati, J.; McLenaghan, R.G. Algebraic invariants of the Riemann tensor in a four-dimensional Lorentzian space. *J. Math. Phys.* **1991**, *32*, 3135–3140. [CrossRef]

26. Carot, J.; Costa, J.D. On the Geometry of Warped Spacetimes. *Class. Quantum Gravity* **1993**, *10*, 461–482. [CrossRef]

27. Santosuosso, K.; Pollney, D.; Pelavas, N.; Musgrave, P.; Lake, K. Invariants of the Riemann tensor for class B warped product spacetimes. *Comput. Phys. Commun.* **1998**, *115*, 381–394. [CrossRef]

28. Lobo, F.S.N. Wormhole Basics. In *Wormholes, Warp Drives and Energy Conditions*; Fundamental Theories of Physics; Lobo, F.S.N., Ed.; Springer: Cham, Switzerland, 2017; Volume 189, pp. 11–33.

29. Brooks, D.; MacCallum, M.A.H.; Gregoris, D.; Forget, A.; Coley, A.; Chavy-Waddy, P.C.; McNutt, D.D. Cartan Invariants and Event Horizon Detection, Extended Version. *Gen. Relativ. Gravit.* **2018**, *50*, 37. [CrossRef]

30. Alcubierre, M. The warp drive: hyper-fast travel within general relativity. *Class. Quantum Gravity* **1994**, *11*, L73–L77. [CrossRef]